HHS Public Access

Author manuscript

Opt Express. Author manuscript; available in PMC 2015 July 01.

Published in final edited form as:

Opt Express. 2009 March 30; 17(7): 5794–5806.

Retention of polarization signatures in SHG microscopy of scattering tissues through optical clearing

Oleg Nadiarnykh and **Paul J. Campagnola***

University of Connecticut Health Center, Center for Cell Analysis and Modeling, Department of Cell Biology, Farmington, CT 06030, USA

Abstract

Polarization responses in Second Harmonic Generation (SHG) imaging microscopy are a valuable method to quantify aspects of tissue structure, and may be a means to differentiate normal and diseased tissues. Due to multiple scattering, the polarization data is lost in turbid tissues. Here we investigate if this information can be retained through the use of optical clearing which greatly reduces the scattering coefficient and increases the corresponding mean free path. To this end, we have measured the SHG intensity as a function of laser polarization and the SHG signal anisotropy in murine tendon and striated muscle over a depth range of 200 microns. We find that the laser polarization is highly randomized in the uncleared tissues at depths corresponding to only 2–3 scattering collisions (50-10 microns). This depolarization of the laser is also reflected in the randomized anisotropy of the SHG signal as it is created over a range of polarization states. In strong contrast, both polarization signatures are significantly retained through ~200 microns of tissue thickness following treatment with 50% glycerol. Moreover, the measured polarization responses for both tendon and striated muscle are consistent with the extent of reduction of the respective scattering coefficients upon clearing. We suggest the method will be applicable to SHG imaging of connective disorders as well as cancer through several hundred microns of extracellular matrix.

1. Introduction

Determining the health of tissues by in vivo imaging could impact diagnosis and monitoring of many diseases in a non-invasive or minimally invasive manner. However, currently used clinical technologies are hampered by insufficient resolution, lack of specificity, or high degree of invasiveness. While significant technological advances have greatly improved the capabilities of ultrasound, MRI, CT, and PET imaging these modalities are practically limited to resolutions of ~ 1 mm. Similarly diffuse optical tomography and photoacoustic tomography are limited to resolutions of ~ 1 mm and 100 microns, respectively. However, much higher spatial resolution (1 micrometer or less) is required to visualize structural changes associated with diseased cells and tissues. For example, it is increasingly recognized that changes in the microscopic tissue structure, e.g. the collagen fibril assembly

*Corresponding author: campagno@neuron.uchc.edu.

OCIS codes: (180.6900) Three-dimensional microscopy; (190.4180) Multiphoton processes; (190.2620) Harmonic generation and mixing; (290.7050) Turbid media; (290.4210) Multiple scattering

in and around tumors, may also be early indicators of disease. To meet this need, we have been implementing Second Harmonic Generation (SHG) microscopy, which visualizes tissue assembly with submicron resolution, as a tool to differentiate normal and diseased states, (e.g. connective tissue disorders or cancers). For example, the type I collagen is abnormally assembled in osteogenesis imperfecta (brittle bone disease) and we found SHG could differentiate diverse tissues such as bone, skin, and tendon using metrics based on intensity comparisons, polarization analysis, and emission directionality.[1, 2] We further showed statistical differentiation in several murine models of muscle disorders based on changes in sarcomere length.[3] SHG has also shown early promise in cancer imaging as a stand alone technique,[4–6] and it also has been implemented in multimodal approaches combining multiphoton excited fluorescence.[7, 8] Given these successes, minimally invasive and truly *in vivo* visualization of tissues may well progress into clinical techniques for assessing disease severity, and monitoring efficacy of treatment.

However, the increased resolution and specificity of multiphoton microscopy techniques comes at the expense of limited imageable penetration depths relative to established clinical modalities which typically image through several mm or cms of tissue. As opposed to this diffuse regime, high resolution microscopy based techniques must operate in the ballistic or quasi-ballistic regimes (a few scattering lengths), where the achievable depth is limited by scattering of both the excitation light and the intrinsically generated signal. With laser excitation in the 800–1000 nm range, typical imaging depths in tissues are approximately 100–300 microns. While this range is not highly limiting for imaging *ex-vivo* physically sliced samples, these depths are inadequate for true *in vivo* applications. Thus it would be highly advantageous to achieve better imaging depth in nonlinear optical microscopy methods in general. It would be additionally powerful for the specific case of SHG to achieve this goal while simultaneously exploiting the power of polarization analysis to obtain detailed structural data about the tissue assembly.

SHG is a vector quantity and has a well-defined polarization governed by the geometrical disposition of source harmonophores within the molecular assembly (i.e. $\chi^{(2)}$ tensor), a property below the resolution of any optical method. We have previously shown how the SHG intensity as a function of laser polarization is related to the pitch angle of the protein helix[9] and that the SHG signal anisotropy is related to the dipole assembly.[10] Moreover, deviations from the normal polarization response will indicate the degree of disorganization of protein structures in diseased tissues.[1]

However performing these measurements in strongly scattering tissues is problematic since each scattering event experienced by both the laser fundamental and SHG wave introduces some depolarization.[11] As a result, structural information encoded in SHG will become increasingly scrambled at increasing tissue depths of greater than one mean free path (MFP) for the fundamental and/or SHG signal. While there have been several papers on SHG polarization analysis, these have either been performed at either superficial depths in tissues or in isolated myofibers or collagen fibers.[9, 12, 13] The evolution of how these SHG responses degrade in tissues for the excitation and signal waves has not yet been reported. To fully exploit the power of SHG it is important to both determine the usable range as well as increase upon this limit for polarization analysis. As we are limited in terms of both

convenient laser sources as well as the biological transparency window in using longer excitation wavelengths, other approaches must be found to increase imaging depths.

To help overcome the inherent depth limitations in turbid tissues while maintaining high resolution coupled with polarization analysis, we will combine SHG imaging with optical clearing.[14] Several researchers have recently employed this method in a variety of optical modalities. In this process, a high refractive index, hyper-osmotic reagent (e.g. glycerol, sugars, or sugar alcohols) is added to the tissue to increase its transparency. Such diverse tissues as skin, [15–18] blood,[19, 20] *dura mater*, [21] gastric tissue,[22] sclera,[23, 24] bone, [25] and muscle[26] have been studied by this process, where the optical imaging modalities have included brightfield microscopy, tissue spectroscopy, OCT, and SHG microscopy. In many cases the penetration depth was increased by several fold. It is widely accepted that a decrease in the reduced scattering coefficient, μ_s', is responsible for this effect, where the optical clearing potential has been defined as ($\mu_s'_{cleared}/\mu_s'_{uncleared}$).[16] As described by Mie theory,[27] this ratio becomes infinite for the case of perfect refractive index matching.[27]

Previously, we investigated the mechanisms and benefits of optical clearing for SHG imaging of tendon and striated muscle.[26, 28] We demonstrated that in muscle optical clearing arises from replacement of intracellular water with glycerol (n=1.47) thus matching the initially lower refractive index of the cytoplasm in the muscle cells (n=1.38) with the higher refractive index of the surrounding collagenous perimysium (n=1.47). In the case of tendon in addition to refractive index matching via interfibrillar water replacement with glycerol, this interfibrillar spacing is increased resulting in a longer mean free path (MFP). In these efforts we measured the bulk optical parameters and performed Monte Carlo simulations of the axial directional (Forward/Backward) and attenuation responses and found the experimentally observed improvement in imaging was consistent with the reduction of μ_s'. [28]

In this paper, we draw upon our previous work and now investigate the efficacy of optical clearing in retaining the SHG polarization responses in skeletal muscle and tail tendon. These are representative highly scattering tissues that we have used in previous investigations of SHG imaging of diseased states.[1, 3] Moreover, both are well-ordered in terms of fiber assembly and well-suited for investigative polarization studies. We find that optical clearing greatly enhances the retention of polarization signatures in these highly scattering tissues relative to the controls, and further that our findings our consistent with the respective measured scattering coefficients. We additionally show that 2–3 scattering collisions is sufficient to significantly randomize the SHG polarization responses in the control tissues.

2. Experimental Methods

2.1. Tissue preparation

The tendon and muscle samples were obtained from adult CD1 mice sacrificed by CO_2 narcosis, in accordance with our approved animal care protocol. To isolate tendon fibrils the skin was pulled from tail, and strips of tendon collagen were carefully detached from bones, and transferred into phosphate buffered saline (PBS). Before imaging tendon was cut into

smaller fragments (0.5cm long). Snips of quadriceps femoris muscles were dissected from lower limbs and sliced on a vibratome into 200 μm horizontal sections. Optical clearing was performed overnight in 50% glycerol-PBS solution.

2.2. SHG microscope

The SHG imaging system consists of a laser scanning unit (Olympus Fluoview 300) mounted on an upright microscope (Olympus BX61), where the excitation source is a mode-locked Titanium Sapphire laser (Coherent Mira). All measurements were taken with a laser fundamental wavelength of 890 nm with average power between 5 and 20 mW at the focal plane. The imaging system simultaneously collects both the forward and the backward components of SHG signal. In the former, a long working distance 40X 0.8 NA water-immersion objective and a 0.9 NA condenser provide excitation and signal collection, respectively. The backward component is collected in a non-descanned configuration. In both geometries, the SHG signal is isolated with a longwave pass dichroic mirror and 10 nm bandpass filters (445 nm). The signals are detected by two identical photon-counting photomultiplier modules (Hamamatsu). The SHG wavelength was confirmed with a fiber optic spectrometer (Ocean Optics). There is no autofluorescence for collagen or skeletal muscle at this excitation wavelength.

The input polarization is controlled by a set of half- and quarter-wave plates, where the latter is used to compensate for ellipticity in the polarization introduced in the beampath. We *de facto* determined the polarization of excitation light at the focal plane by matching SHG maxima and minima to those previously measured for linear (myofibrils) and spherical (circular cells) specimens. To perform the dependence of the laser polarization at fixed focal planes we simultaneously recorded forward and backward SHG images, while rotating the plane of polarization at 5° steps at high zoom (4×). Changing the polarization by either the half-wave plate or specimen rotation produced similar results. We adapted both acquisition channels for analysis of the polarization of the resulting SHG signals by addition of collimation lenses and Glan laser polarizers. The initial polarization was set to the maximum of the laser polarization response (45 degrees with respect to the fiber axis).[9] Images were taken with the analyzing polarizers oriented parallel and orthogonal relative to the laser polarization to calculate the resulting signal anisotropy, β. Using membrane stained spherical neuroblastoma cells we obtained a correction factor of 0.08 for the anisotropy measurement to account for minor losses of polarization introduced by the dichroic mirror in the collection path. For both polarization responses, this analysis is performed for single fibrils or small groups of parallel-oriented fibrils with ImageJ software (http://rsb.info.nih.gov/ij).

3. Results

3.1 Laser polarization dependence of the SHG intensity from tendon

First, we investigate the dependence of the SHG intensity on the laser polarization for uncleared and cleared tendon at different tissue depths. For collagen fibrils, the SHG intensity profile with respect to angle with input polarization, θ, exhibits a angular dependence with maxima at 45 and 135 degrees and local minima at 0, 90, and 180 degrees,

respectively.[9] The results for control tendon are shown in Fig. 1, where the top panels display representative optical sections for 0, 45, and 90 degrees for 5 and 45 microns into the tissue. The bottom panel plots the intensity dependence on the laser polarization over 180 degrees for these depths. For the 5 um depth (blue squares) the polarization profile is the same as we have previously reported.[9] By contrast, the angular dependence is essentially completely lost at a depth of only 45 μm from the tendon surface (red circles). This arises because the laser fundamental gets depolarized by scattering events prior to its arrival at the focal plane, which is equivalent to probing the sample with random polarization. At the laser excitation wavelength of 900 nm, the scattering coefficient μ_s is 400 cm^{-1} or equivalently the MFP=25 microns.[28] Thus, the laser photons on average will experience two scattering events which results in significant depolarization.

According to our previous findings the reduction of primary filter effect (or scattering of the laser fundamental) in general defines the imaging depth[2] and additionally dominates the observed improvement in imaging depth as a result of optical clearing.[28] Here we investigate the extent that the reduction of scattering through optical clearing results in retention of polarization dependence. To this end we performed the same experiment on tendon cleared overnight in 50% glycerol, and show the results in Fig. 2, where representative optical sections are shown for the 100 micron depth at 0, 45, and 90 degrees. In this case we obtained very similar polarization profiles at depths of 10 um (black squares) and 100 um (red circles). Based on our previous measurements, the scattering coefficient is reduced by nearly 2 orders of magnitude from 400 cm^{-1} to 3 cm^{-1} at 890 nm.[28] Thus the MFP is 3 mm and on average the laser will experience no scattering events in 100 microns of depth and, therefore, the fundamental retains its initial polarization state. We note that the overall shape of the polarization dependence is similar but not identical to that of the uncleared tissue in Fig 1. The maxima are flatter and the minimum sharper for the cleared tissue. This may arise from a change in the collagen structure upon glycerol treatment, where possible mechanisms have been discussed by Yeh and coworkers.[29] However, these responses are compared self-consistently in the same tissue at different depths as the refractive index away from the surface will be the same.

3.2 Tendon SHG anisotropy

The second polarization response to be examined is the SHG signal anisotropy, which relates to the alignment of dipoles within the focal volume. The polarization state of the SHG signal can be described by its anisotropy parameter β according to Eq. 1:

$$\beta = \frac{I_{par} - I_{orth}}{I_{par} + 2I_{orth}} \quad (1)$$

where I_{par} and I_{orth} are components of SHG intensity polarized parallel and orthogonal with respect to the polarization of excitation laser. The signal anisotropy ranges between −0.5 (all dipoles aligned perpendicular to the laser polarization), and β=1.0 where all the dipoles are aligned with themselves and with the laser polarization. The special case of β=0 corresponds to the isotropic condition where $I_{par} = I_{orth}$. We will use this scenario to describe the complete depolarization of the SHG signal by scattering events during its propagation through turbid media. Here we will investigate how β evolves with increasing depth (and

scattering) for tendon, and further, if it can be retained through optical clearing. This is an important consideration as loss of the SHG anisotropy reduces the information content that SHG provides in comparing differences in tissue structure.

We perform this analysis for both the forward and backward SHG components, as the latter will be the most relevant for in vivo applications. The detected backward SHG is a super-position of direct quasi-coherent emission[30] and a multiple scattered incoherent component. In general, the measured signal in turbid tissue results from both contributions,[31] where the relative magnitudes depend on the morphology of the tissue assembly as well as the bulk optical parameters. We have determined that the initial emission directionality, F_{SHG}/B_{SHG}, is ~ 5:1 in tendon (un-published results).

To this end, we probed the samples at preset z-positions with fixed vertically polarized laser excitation, and analyzed those tendon fibrils aligned at 45 degrees where the SHG intensity has maximum according to profile in Fig. 1. Each optical section was imaged twice with the Glan polarizers oriented parallel and then perpendicular to the laser polarization. The resulting depth dependence of both the forward and backward collected channels of the anisotropy parameter for tendon over the tendon thickness of 60 microns is shown in Fig. 3.

The data show that for both channels, the anisotropy decreases with increasing depth into the tissue. We can explain these trends by consideration of the initial directionality, and the effects of depolarization of the laser and resulting SHG signal. The backward anisotropy is largest at the top surface, where it is dominated by the direct emitted backward component, where these photons only need to propagate a short distance to the tissue top surface and be collected. Analogously, the backward anisotropy is the smallest near the bottom surface, where photons will have the highest probability of being scattered and depolarizing before being collected (for both direct backward emission and multiply scattered forward directed photons). We also note the forward anisotropy gradually decreases with increasing depth into the tissue. It might be anticipated that the forward anisotropy would increase near the bottom surface as the propagation length for the SHG decreases. However for tendon, the scattering coefficients for the laser fundamental and SHG wavelengths are similar at 400 and 510 cm^{-1}, respectively. Thus the significant scattering depolarization of laser will also serve to randomize the SHG anisotropy, as the SHG will be produced by several polarization states (although not equally). This is analogous to our previous finding that primary filter effect dominates the achievable image depth in several tissues (dermis, tendon and muscle), and does here as well in terms of defining the net SHG signal anisotropy. We lastly note that all the forward values are close to the isotropic case of $\beta=0$, with the maximum of ~0.2. Tendon, in the absence of scattering could have a β close to 1.0 due to the highly regular alignment of the fibrils.

A strikingly different behavior is observed in cleared tendon (blue squares) shown in Figure 4 (red squares are the forward data from Fig 3). Here, the forward signal anisotropy increases from 0.3 for SHG originated at the top to 0.85 for SHG excited at the bottom exit from the 110-μm thick sample. We note that the total thickness nearly doubled relative to the control due to expected swelling that occurs during optical clearing.[28] The result is consistent with the significant reduction of the laser depolarization as described above as

well as the 20-fold reduction of scattering coefficient at SHG wavelength from 510 cm^{-1} to 27 cm^{-1}. Thus in the limit of no laser depolarization, the SHG anisotropy increases as the propagation length to the tissue exit is decreased. While this thickness is less than one MFP, a fraction of the SHG photons will experience one scattering event which reduces the anisotropy below the maximum value. Similar trends are seen in the backward SHG (b), where the absolute β values are lower since most of the backward signal arises from scattering of the forward SHG, as opposed to the forward SHG arising from directly generated emission. We note that the anisotropy limit for the forward at the top and the backward at the bottom of the tissue are similar (~0.3). This arises because the propagation pathlengths of the photons are similar (i.e. forward top-bottom and backward bottom-top, respectively). We previously reported a similar finding of increasing anisotropy through 500 microns in *Acetobacter* cellulose (without clearing) which is characterized by a small primary and moderate secondary filter effect (μ_s ~12 cm^{-1} and μ_s ~75 cm^{-1} respectively). [31]

3.3 Laser polarization dependence of the SHG intensity from striated muscle

As reported by several researchers, the SHG from striated muscle arises from myosin and has characteristic dependence on the laser polarization, where the angular dependence of the SHG intensity exhibits maxima at 45 and 135 degrees and a minimum at 90 degrees.[9, 13] Here we investigate how this response degrades at increasing depths into muscle tissue. Data for the control muscle is shown in Figure 5, along with the cleared data at depths of 10, 100, and 180 microns. We note the input polarization profile is largely randomized at the depth of 100 μm into the muscle tissue. The scattering coefficient at 890 nm for striated muscle is 285 cm^{-1}, thus the MFP is ~35 microns, corresponding to approximately 3 scattering events. This randomizes the laser polarization as we observed in tendon (Figure 1). Upon treatment with 50% glycerol, the polarization profile is preserved through 100 μm of the optically cleared muscle. Some depolarization is evident at 180 μm depth as the amplitude of the curve goes down, especially in the 0 to 45 degrees range where peak-to-valley difference (i.e., dynamic range) is inherently lower. These observations are consistent with the previously measured 10-fold decrease in the scattering coefficient to 29 cm^{-1} (MFP ~340 microns) in cleared muscle, where no depolarization will occur into 100 microns of tissue thickness (<<MFP) and limited effect in 180 microns (<1 MFP).

3.4 SHG anisotropy from striated muscle

In analogy to tendon, we measured the SHG anisotropy with increasing depth for control and optically cleared tendon (Fig. 6). The fibers were oriented at 45 degrees relative to the vertical laser polarization to achieve the greatest intensity. Unlike tendon, muscle tissue did not produce a monotonic depth-dependence of the SHG anisotropy, due to differences in the tissue assembly. Specifically, tendon has uniformly aligned collinear fibrils throughout the whole fiber, where any bending or change in direction occurs gradually with depth. In contrast, the muscle tissue is comprised of multiple cells (~20–50 microns in diameter) wrapped in a thin (~2 μm) layer of collagenous perimysium. The boundary between the muscle cells causes a change in birefringence that will change the polarization of the scattered photons. As discussed by Wang the depolarization in a birefringent medium does not occur isotropically but depends on the initial polarization, the birefringence, and shape of scatterers.[32] In the current case, the anisotropy displayed oscillatory behavior at these

locations. We previously observed the effects of these local changes in the axial attenuation of the SHG in muscle, where a curvature in the response occurred at the cell boundaries.[26] Additionally, artifacts are introduced by slicing at the top and bottom surfaces of the samples, whereas tendon samples were imaged intact. All these factors combined result in abrupt changes in local fibril alignments at and in the vicinity of all the interfaces. Therefore, in Figure 6 we present the average SHG signal anisotropy values from the middle regions of two muscle cells in the biopsy at average depths of 50 and 180 microns. Similar to tendon, the uncleared tissue shows significant depolarization at the top and bottom of the tissue. There is a slight increase in the anisotropy at the bottom exit as the laser depolarization of the laser is not as strong as observed in tendon (based on the respective scattering coefficients at 890 nm).

The signal from the cleared muscle shows a considerably higher degree of polarization, which trends higher for SHG emitted closer to the exit from the sample (~0.4). As shown above in Fig. 5, the laser does not experience significant depolarization in the cleared tissue, as the depth at 180 microns corresponds to ~0.5 MFP. The scattering coefficient for the SHG wavelength decreases from 500 to 75 cm^{-1} (MFP~133 microns). Thus we observed substantial but not complete retention of the anisotropy due to approximately 0.5 and 1.5 scattering events of the laser and SHG signal, respectively.

4. Discussion

Here we have systematically investigated the evolution of SHG polarization responses in the representative highly scattering tissues of murine tendon and striated muscle. While SHG polarization analysis has been previously described, the nature of how these polarization signatures degrade in scattering tissues has not been reported. Stolller et al saw a loss of the polarization dependence in tendon (as in Fig. 1) at 30 microns but did not address the origin of the response.[33] Having measured the scattering coefficients,[28] we now point out that 2–3 scattering events for laser photons result in significant depolarization, leading to a nearly randomized dependence of the SHG intensity on the initial polarization. This depolarization is also evident in the SHG anisotropy, as the initial anisotropy will be somewhat randomized due to the randomized laser polarization. Thus in analogy to our previous efforts that showed the primary filter effect predominantly determined the achievable imaging depth,[1, 28] the polarization purity of the laser at the focal plane dominates both SHG polarization responses. In fluorescence confocal imaging of fluorescent beads, Foster showed that depolarization occurred within several mean free paths.[34] We find significant depolarization within fewer scattering events. This may be due to the second order nature of the SHG, where the polarization dependence will be more sensitive to the initial polarization state of the laser.

We find that the polarization dependences (laser polarization and SHG anisotropy) are significantly retained in both tendon and striated muscle through optical clearing. The extent that these properties are preserved is consistent with our measured values of the respective scattering coefficients (un-cleared and cleared) at the fundamental and SHG wavelengths.[28] Thus, the process can be performed on tissues with some a priori knowledge of the improvement that can be achieved (if the scattering coefficients are known). The ability to

measure these polarization attributes in highly scattering tissues is important as they are directly related to tissue structure, and may be different in normal and diseased tissues. For example, this may be essential in imaging tumors through several hundred microns to determine the extent of invasion into the ECM. We note that we have previously shown that clearing does not significantly disrupt the tissue structure in striated muscle[26] and that in a-cellular collagenous tissues, the process is essentially reversible.[28]

We recognize that there still might be potential safety issues with the use of clearing agents in vivo both in terms of toxicity and exposure time. As described above, both tendon and muscle swell upon treatment with 50% glycerol. Other researchers have reported shrinking under glycerol treatment due to de-hydration in the inter-celullar space.[35] The difference in behavior is likely due to the cellularity of the tissue structure. For example, tendon is completely a-cellular and skeletal muscle consists of tightly packed supercells wrapped with collagen and essentially no inter-cellular space for hydration. In contrast, gastric tissue has highly dynamic water flow. We further note that development of optical clearing methods[36] is an active area of research and new agents or delivery schemes may be found that are suitable for in vivo use. However, the ability to gain further knowledge into tissue structure may provide insight into changes that occur during connective tissue disorders and cancer. Moreover, imaging ex vivo tissues through optical clearing offers advantages over standard histology. Sections for histology require significant preparation in terms of fixing, imbedding in paraffin, and then slicing, where by contrast through SHG imaging and optical clearing, much thicker sections (~200 microns) can be used. As a consequence we can obtain much more data from one section than possible by~20 thin histological sections. Thus optical clearing coupled with SHG polarization analysis is a powerful method even if it is ultimately limited to ex vivo applications.

5. Conclusions

In this work we investigated the effect of optical clearing on polarization properties of SHG emission from highly scattering muscle and tendon samples. To this end, we measured the dependence of SHG intensity on the laser polarization angle and SHG signal anisotropy at different depths. We find that in untreated tissues, based on our measured bulk optical parameters, the polarization signatures are highly randomized in 2–3 scattering events. In cleared tissues, we found that the SHG polarization information is retained in ~200 μm-thick samples, where these effects are consistent with the reduction of the scattering coefficients (and corresponding mean free paths). These findings have significance for probing tissue structure through polarization analysis at increased depths relative to the superficial depths possible of un-treated tissues. While we demonstrated retention of polarization attributes through optical clearing for the specific case of SHG imaging, this method could be applied to other polarization sensitive contrast modalities like fluorescence third harmonic generation, coherent anti-Stokes Raman scattering, and optical coherence tomography.

Acknowledgments

We gratefully acknowledge support under NIH EB01842 and helpful discussions with Dr. Ron LaComb.

References and links

1. Nadiarnykh O, Plotnikov S, Mohler WA, Kalajzic I, Redford-Badwal D, Campagnola PJ. Second Harmonic Generation imaging microscopy studies of Osteogenesis Imperfecta. J. Biomed. Opt. 2007; 12:051805. [PubMed: 17994883]
2. Lacomb R, Nadiarnykh O, Campagnola PJ. Quantitative SHG imaging of the diseased state Osteogenesis Imperfecta: Experiment and Simulation. Biophys J. 2008; 94:4104–4104.
3. Plotnikov SV, Kenny A, Walsh S, Zubrowski B, Joseph C, Scranton VL, Kuchel GA, Dauser D, Xu M, Pilbeam C, Adams D, Dougherty R, Campagnola PJ, Mohler WA. Measurement of muscle disease by quantitative second-harmonic generation imaging. J. Biomed. Opt. 2008; 13:044018. [PubMed: 19021346]
4. Brown E, McKee T, diTomaso E, Pluen A, Seed B, Boucher Y, Jain RK. Dynamic imaging of collagen and its modulation in tumors in vivo using second-harmonic generation. Nat. Med. 2003; 9(6):796–800. [PubMed: 12754503]
5. Provenzano PP, Eliceiri KW, Campbell JM, Inman DR, White JG, Keely PJ. Collagen reorganization at the tumor-stromal interface facilitates local invasion. BMC Med. 2006; 4:38. [PubMed: 17190588]
6. Lin SJ, Jee SH, Kuo CJ, Wu RJ, Lin WC, Chen JS, Liao YH, Hsu CJ, Tsai TF, Chen YF, Dong CY. Discrimination of basal cell carcinoma from normal dermal stroma by quantitative multiphoton imaging. Opt. Lett. 2006; 31(18):2756–2758. [PubMed: 16936882]
7. Cicchi R, Massi D, Sestini S, Carli P, De Giorgi V, Lotti T, Pavone FS. Multidimensional non-linear laser imaging of Basal Cell Carcinoma. Opt. Express. 2007; 15(16):10135–10148. [PubMed: 19547362]
8. Skala MC, Riching KM, Bird DK, Gendron-Fitzpatrick A, Eickhoff J, Eliceiri KW, Keely PJ, Ramanujam N. In vivo multiphoton fluorescence lifetime imaging of protein-bound and free nicotinamide adenine dinucleotide in normal and precancerous epithelia. J. Biomed. Opt. 2007; 12:024014. [PubMed: 17477729]
9. Plotnikov SV, Millard AC, Campagnola PJ, Mohler WA. Characterization of the Myosin-based source for second-harmonic generation from muscle sarcomeres. Biophys J. 2006; 90:693–703. [PubMed: 16258040]
10. Campagnola PJ, Millard AC, Terasaki M, Hoppe PE, Malone CJ, Mohler WA. 3-Dimesional High-Resolution Second Harmonic Generation Imaging of Endogenous Structural Proteins in Biological Tissues. Biophys. J. 2002; 82:493–508. [PubMed: 11751336]
11. Moscoso M, Keller JB, Papanicolaou G. Depolarization and blurring of optical images by biological tissue. J. Opt. Soc. Am. A. 2001; 18:948–960.
12. Sun C-W, Wang C-Y, Yang CC, Kiang Y-W, Hsu I, Lin C-W. Polarization gating in ultrafast-optics imaging of skeletal muscle tissues. Opt. Lett. 2001; 26:432–434. [PubMed: 18040344]
13. Chu S-W, Chen S-Y, Chern G-W, Tsai T-H, Chen Y-C, Lin B-L, Sun C-K. Studies of (2)/(3) Tensors in Submicron-Scaled Bio-Tissues by Polarization Harmonics Optical Microscopy. Biophys. J. 2004; 86:3914–3922. [PubMed: 15189888]
14. Tuchin, V. Optical Clearing of Tissues and Blood. Bellingham, WA: SPIE Press; 2006. Vol. PM 154.
15. Khan MH, Choi B, Chess S, Kelly KM, McCullough J, Nelson JS. Optical clearing of in vivo human skin: Implications for light-based diagnostic imaging and therapeutics. Lasers Surg. Med. 2004; 34:83–85. [PubMed: 15004816]
16. Khan M, Choi B, Chess S, McCullough J, Kelly K, Nelson JS. The use of topically applied chemical agents for optical clearing of skin to improve diagnostics and laser therapeutic applications. Lasers Surg. Med. 2004:17–17.
17. Vargas G, Chan EK, Barton JK, Rylander HG 3rd, Welch AJ. Use of an agent to reduce scattering in skin. Lasers Surg. Med. 1999; 24:133–141. [PubMed: 10100651]
18. Jiang JY, Boese M, Turner P, Wang RKK. Penetration kinetics of dimethyl sulphoxide and glycerol in dynamic optical clearing of porcine skin tissue in vitro studied by Fourier transform infrared spectroscopic imaging. J. Biomed. Opt. 2008; 13:021105. [PubMed: 18465954]

19. Tuchin VV, Xu XQ, Wang RK. Dynamic optical coherence tomography in studies of optical clearing, sedimentation, and aggregation of immersed blood. Applied Optics. 2002; 41:258–271. [PubMed: 11900442]
20. Xu XQ, Yu LF, Chen ZP. Optical clearing of flowing blood using dextrans with spectral domain optical coherence tomography. J. Biomed. Opt. 2008; 13:021107. [PubMed: 18465956]
21. Bashkatov AN, Genina EA, Sinichkin YP, Kochubey VI, Lakodina NA, Tuchin VV. Glucose and mannitol diffusion in human dura mater. Biophys. J. 2003; 85(5):3310–3318. [PubMed: 14581232]
22. Xu XQ, Wang RK, Elder JB. Optical clearing effect on gastric tissues immersed with biocompatible chemical agents investigated by near infrared reflectance spectroscopy. J. Phys. D. 2003; 36:1707–1713.
23. Genina EA, Bashkatov AN, Sinichkin YP, Tuchin VV. Optical clearing of the eye sclera in vivo caused by glucose. Quantum Electronics. 2006; 36:1119–1124.
24. Ghosn MG, Carbajal EF, Befrui NA, Tuchin VV, Larin KV. Differential permeability rate and percent clearing of glucose in different regions in rabbit sclera. J. Biomed. Opt. 2008; 13:021110. [PubMed: 18465959]
25. Schulmerich MV, Cole JH, Dooley KA, Morris MD, Kreider JM, Goldstein SA. Optical clearing in transcutaneous Raman spectroscopy of murine cortical bone tissue. J. Biomed. Opt. 2008; 13:021108. [PubMed: 18465957]
26. Plotnikov S, Juneja V, Isaacson AB, Mohler WA, Campagnola PJ. Optical clearing for improved contrast in second harmonic generation imaging of skeletal muscle. Biophys J. 2006; 90(1):328–339. [PubMed: 16214853]
27. Tuchin VV. Optical clearing of tissues and blood using the immersion method. J. Phys D. 2005; 38:2497–2518.
28. LaComb R, Nadiarnykh O, Carey S, Campagnola PJ. Quantitative SHG imaging and modeling of the optical clearing mechanism in striated muscle and tendon. J. Biomed. Opt. 2008; 13:021109. [PubMed: 18465958]
29. Yeh AT, Hirshburg J. Molecular interactions of exogenous chemical agents with collagen--implications for tissue optical clearing. J Biomed. Opt. 2006; 11:014003. [PubMed: 16526880]
30. Lacomb R, Nadiarnykh O, Townsend SS, Campagnola PJ. Phase Matching considerations in Second Harmonic Generation from tissues: Effects on emission directionality, conversion efficiency and observed morphology. Opt. Comm. 2008; 281:1823–1832.
31. Nadiarnykh O, LaComb RB, Campagnola PJ, Mohler WA. Coherent and incoherent SHG in fibrillar cellulose matrices. Opt. Express. 2007; 15:3348–3360. [PubMed: 19532576]
32. Wang X, Wang LV. Propagation of polarized light in birefringent turbid media: a Monte Carlo study. J. Biomed. Opt. 2002; 7:279–290. [PubMed: 12175276]
33. Stoller P, Kim B-M, Rubinchik AM, Reiser KM, Da Silva LB. Polarization-dependent optical second-harmonic imaging of a rat-tail tendon. J.Biomed. Opt. 2001; 7:205–214. [PubMed: 11966305]
34. Bigelow CE, Foster TH. Confocal fluorescence polarization microscopy in turbid media: effects of scattering-induced depolarization. J. Opt. Soc. Am. A. 2006; 23:2932–2943.
35. Wang RKK, Xu XQ, He YH, Elder JB. Investigation of optical clearing of gastric tissue immersed with hyperosmotic agents. IEEE J. Select. Top. Quantum Electron. 2003; 9:234–242.
36. Yoon J, Son T, Choi EH, Choi B, Nelson JS, Jung B. Enhancement of optical skin clearing efficacy using a microneedle roller. J. Biomed. Opt. 2008; 13:021103. [PubMed: 18465952]

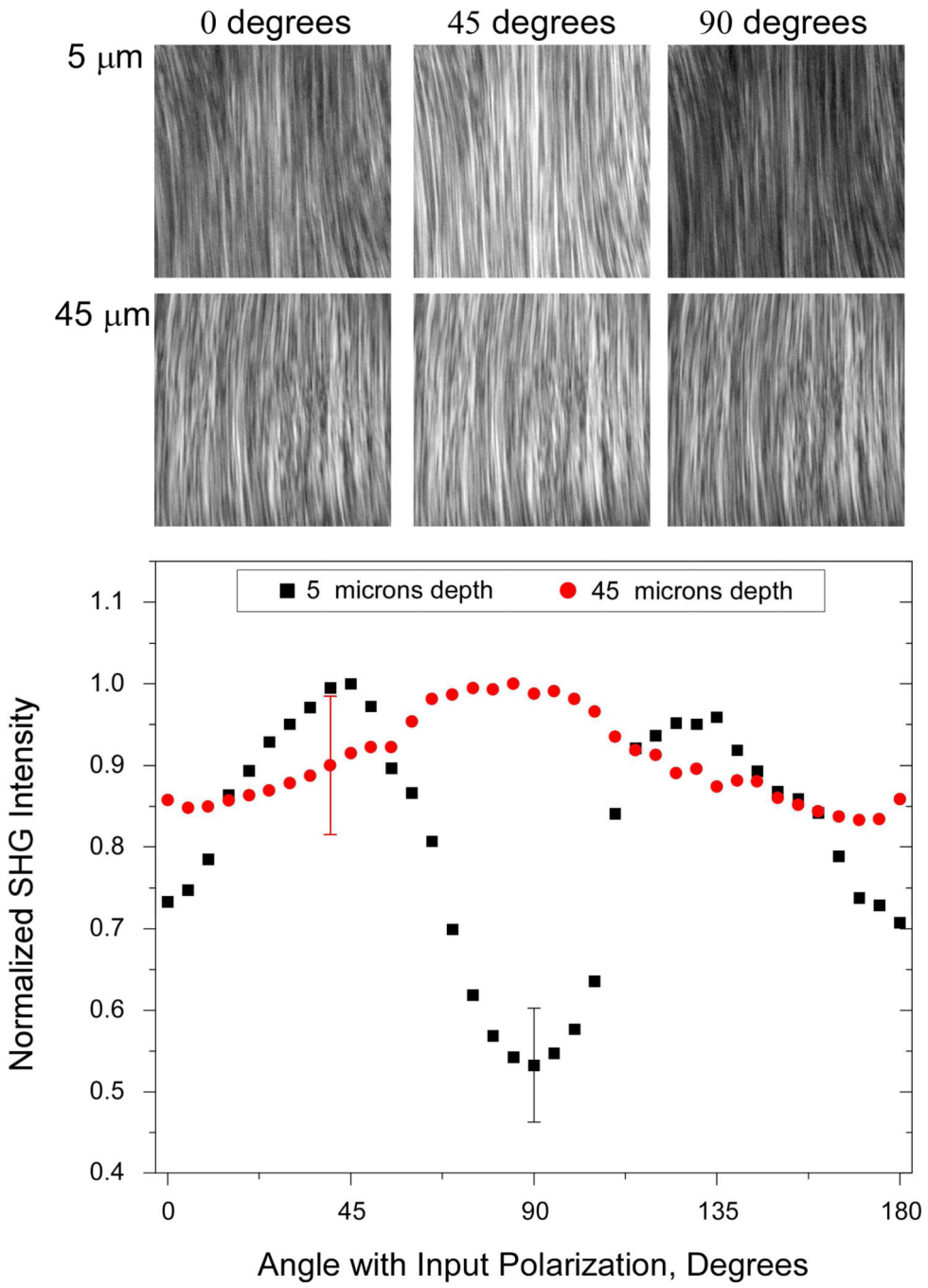

Fig. 1.

Angular dependence of the forward SHG intensity from control tendon at depths of 5 and 45 microns. Representative optical sections at several polarization angles are shown in the top panels. Representative error bars (standard error) are given for one laser polarization for each depth.

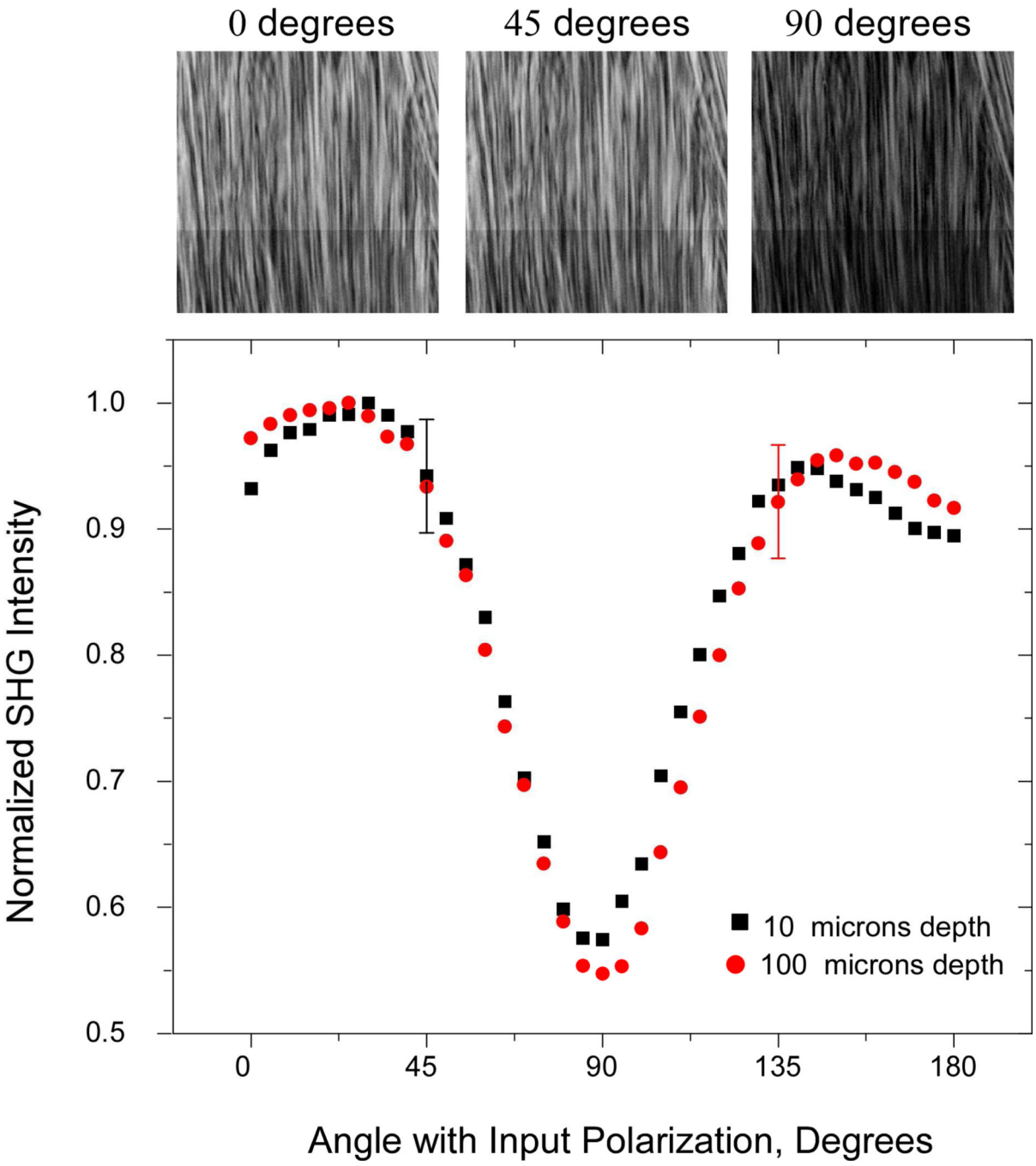

Fig. 2.

Angular dependence of the forward SHG intensity from optically cleared tendon at 10 (black squares) and 100 (red circles) micron depths. Representative optical sections for 100 microns are shown in the top panel Representative error bars (standard error) are given for one laser polarization for each depth.

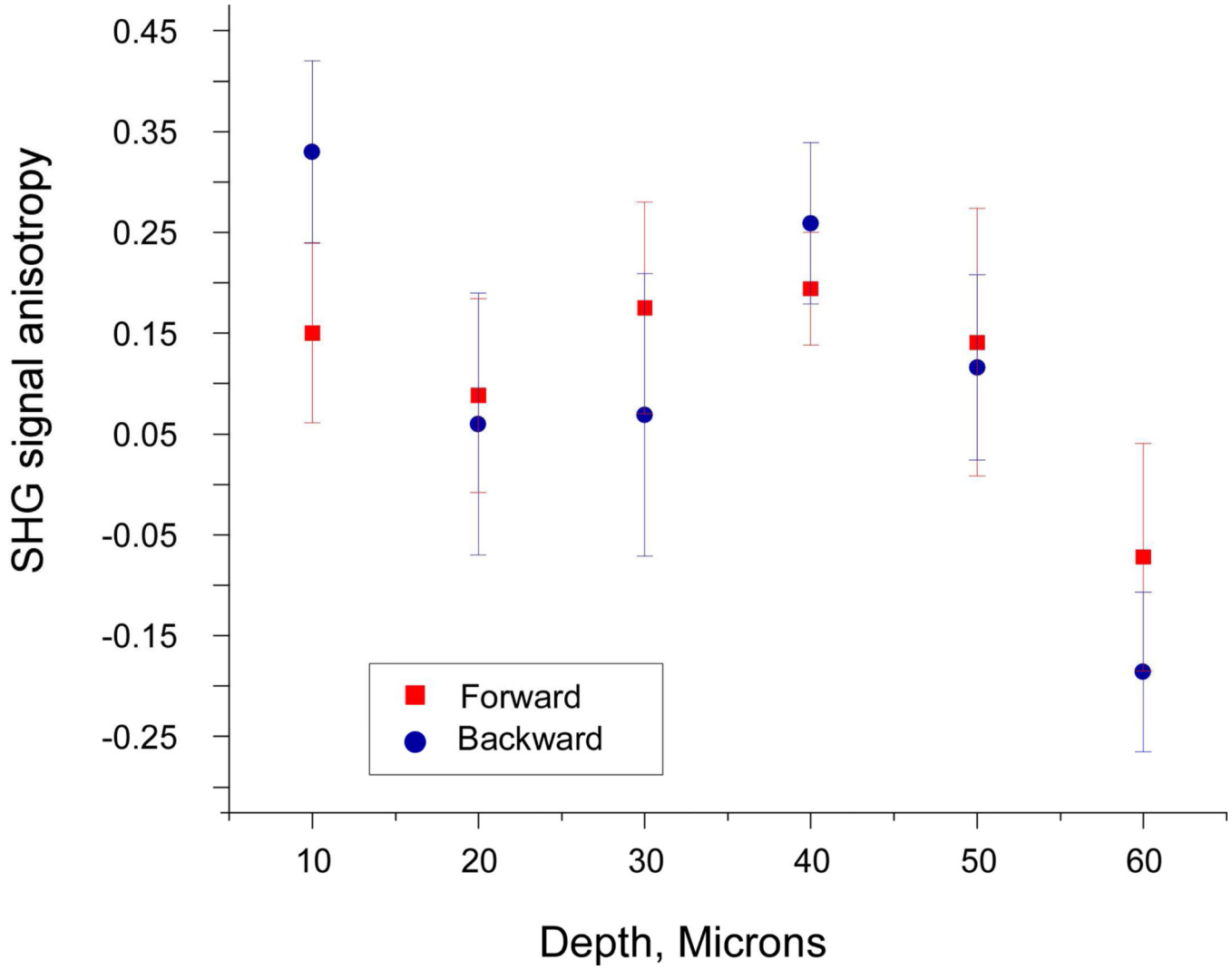

Fig. 3.
SHG anisotropy β measured for forward (red squares) and backward (blue circles) for control tendon.

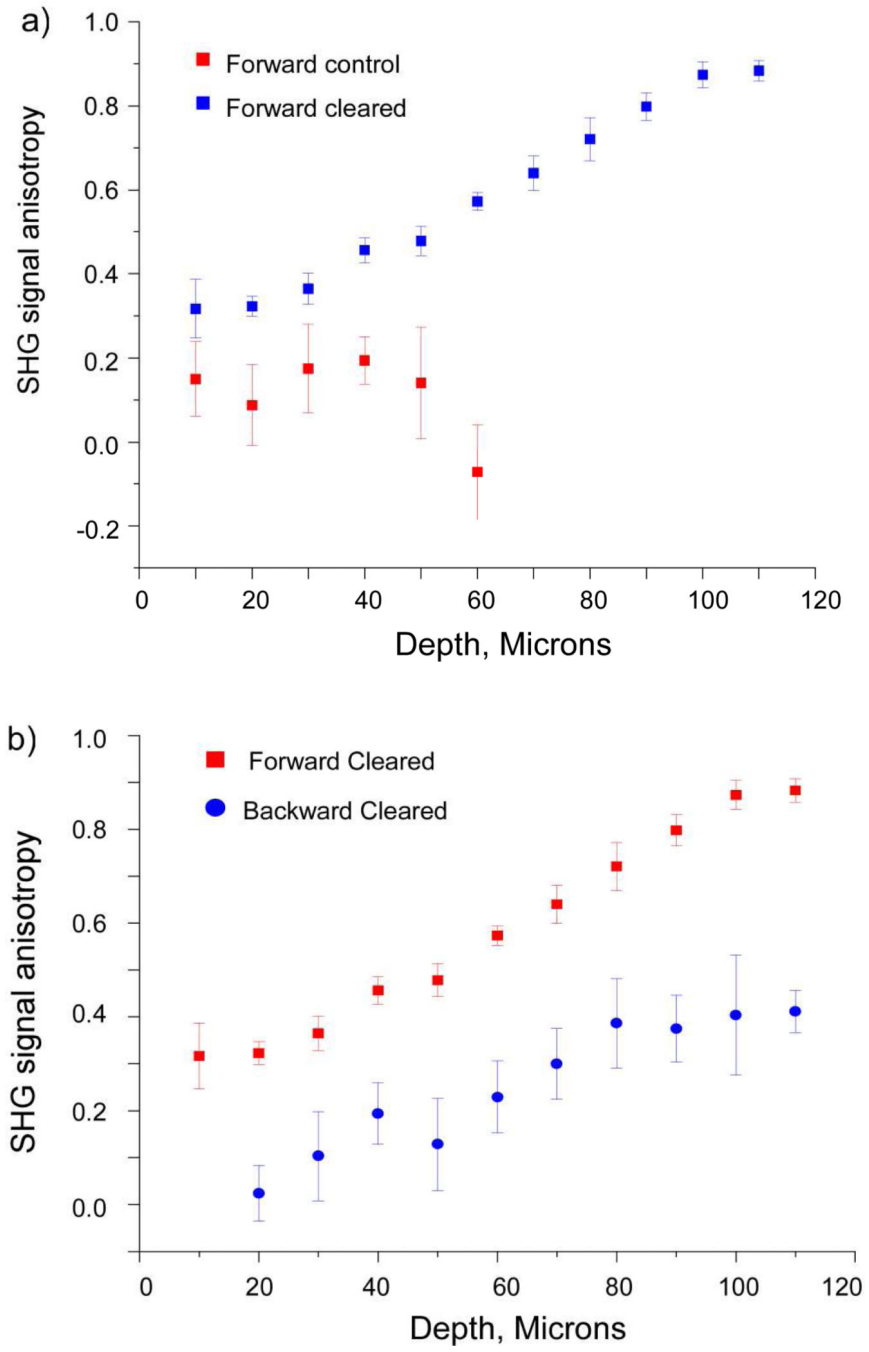

Fig. 4.

(a) Forward SHG anisotropy β measured for forward SHG from control (red squares) and cleared (blue squares) tendon. (b) Forward (red squares) and backward (blue circles) anisotropy in cleared tendon.

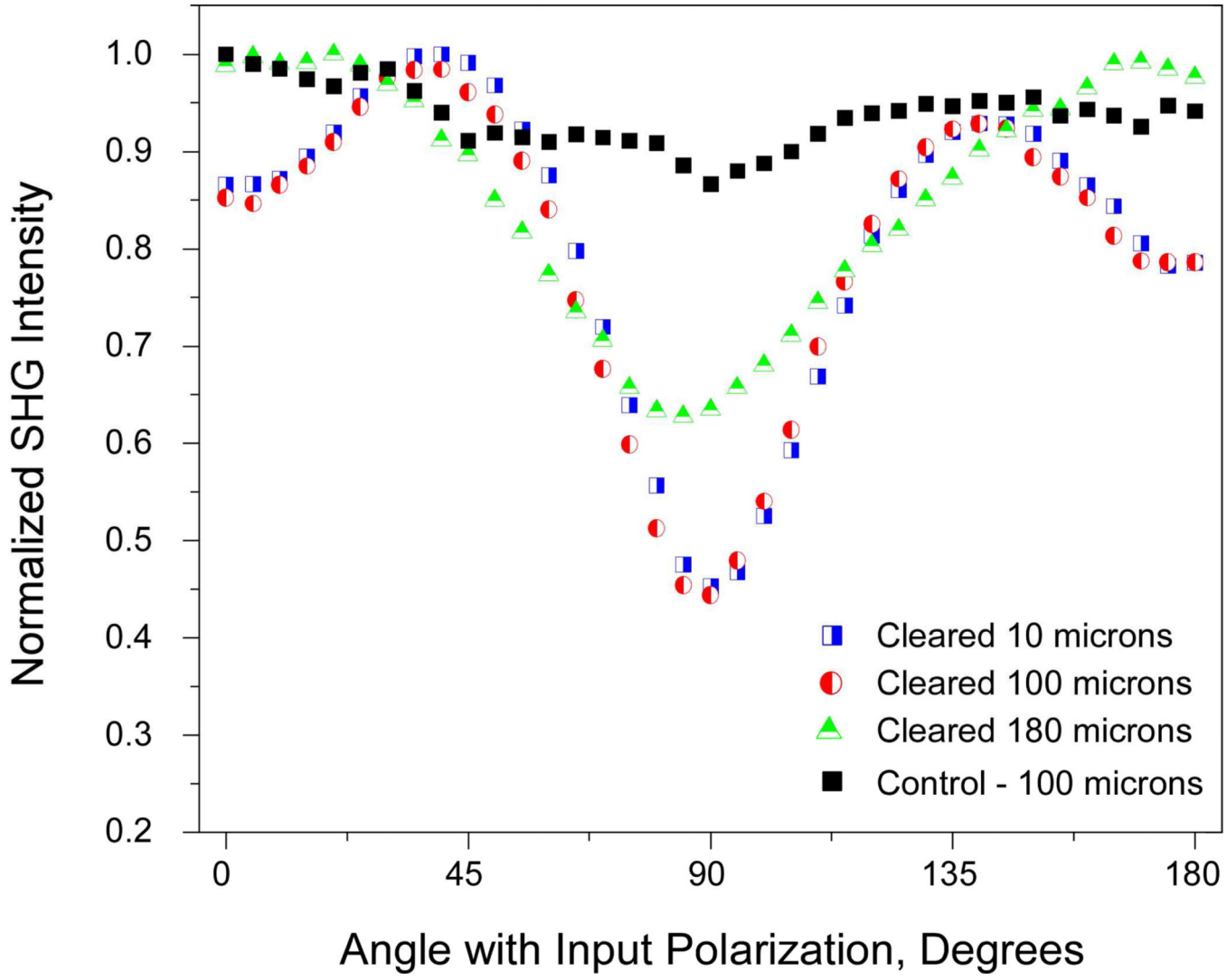

Fig. 5.

Angular dependence of the forward SHG from control and optically cleared muscle at different depths up to 180 microns.

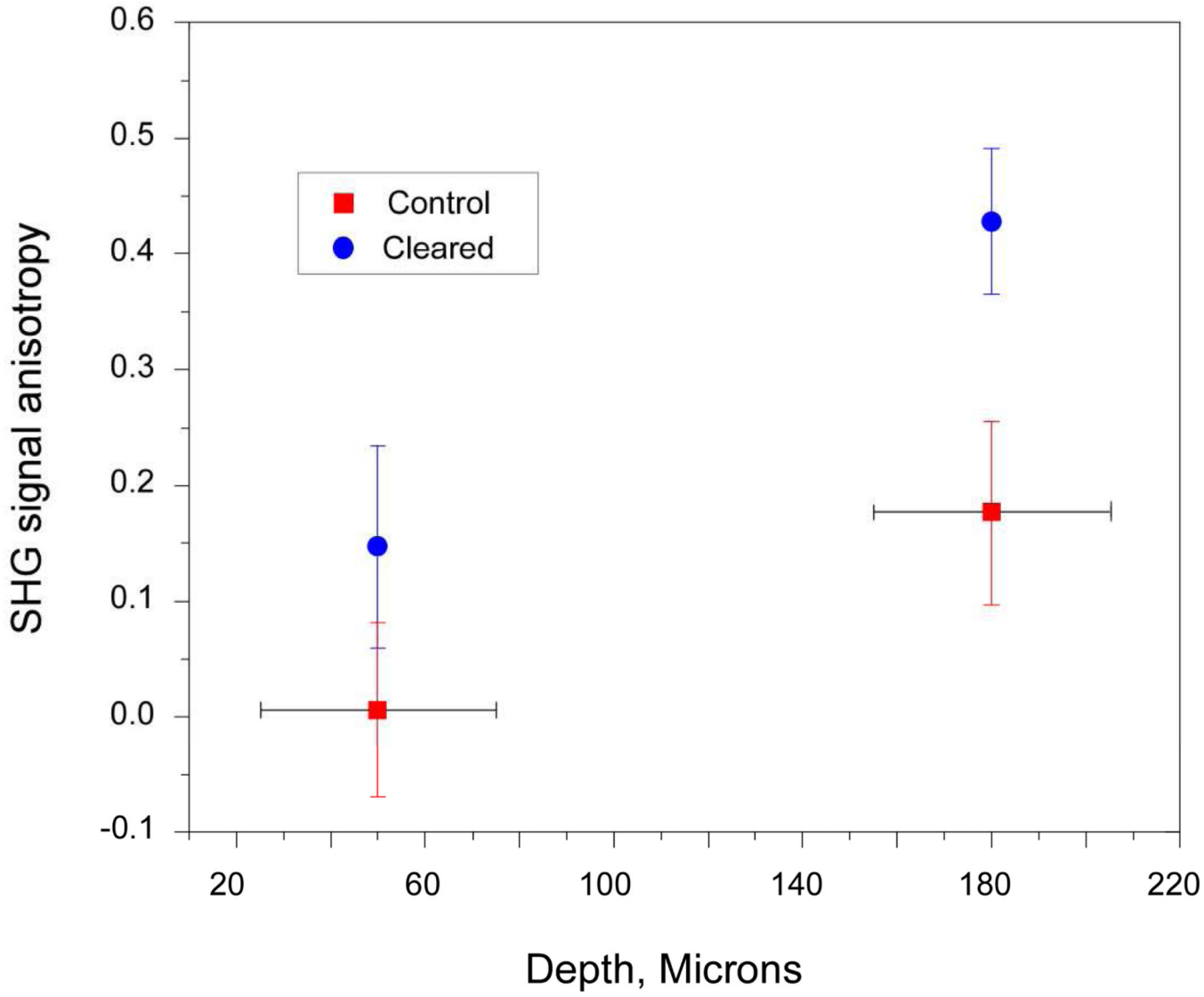

Fig. 6.

SHG anisotropy β calculated for forward SHG from control (red squares) and cleared (blue circles) muscle samples. The data is presented at two depths corresponding to the middle regions of two muscle cells at 50 and 180 microns.